Effect of a Staged End-Cap Chamber Deployment on MDT System Performance*

Daniel S. Levin, Bing Zhou

April 28, 2000

Department of Physics, University of Michigan

Abstract

This paper evaluates the muon track reconstruction and momentum resolution when specific arrays of mid-section (EEL/S) or outer end-cap chambers (EOL/S) are not deployed, compared to a baseline configuration having a full complement of chambers. The effect on Higgs physics for the 4-muon decay channel is also assessed. If either of the above complete chamber sets are not in place the momentum resolution, over the P_t range from 20-500 GeV and corresponding rapidity ranges $1.0 < \eta < 1.37$ and $1.34 < \eta < 2.7$ is degraded. The number of unreconstructed tracks and the occupancy of non-Gaussian tails increases significantly. This resolution change results in a 15% wider mass peak for Higgs masses near 150 GeV . The increased background admitted by a wider peak could erode a possible signal into marginality. With only a part of the outer chambers absent (EOL/S chambers 4,5,6) the degradation of resolution for $P_t \sim 20$ GeV is small and the corresponding effect on the 150 GeV Higgs mass sensitivity is only slightly significant.

*ATL-COM-MUON-2000-005

1 Introduction

A recent Lehmann review has forwarded a recommendation that US ATLAS adhere to its established commitment to construct 240 MDT chambers as described in the Project Managment Plan [3] and guarantee that the detector will be ready for physics measurements by the scheduled beam of July 2005. This production quota falls short of the full complement of MDT chambers included in the baseline design outlined in the PMP [4] and the TDR. The baseline design specifies construction of 320 end-cap inner (EIL/S) and middle section (EML/S) chambers. Outer chambers comprising the outer station (EOL/S) in end-cap towers are to be constructed in Protvino, Russia. If less than the full complement of end-cap chambers is to be installed by the beam turn-on it becomes necessary to explore the impact of a staged deployment on momentum resolution, acceptance and physics potential and to determine which chambers' absence would minimally degrade physics performance.

To address these issues we have generated a series of Monte Carlo simulations and track reconstructions with specific sets of chambers excised. Clearly, exploration of all possible chamber configurations is time consuming and not expedient. We know from the outset that: 1) on average, the magnetic field integral is largest between the inner and outer sets of chambers while it is very small between the middle and outer stations. It is therefore expected that their removal would have less impact on momentum resolution than removal of inner or middle chambers. 2) If inner or middle chambers are initially omitted their inclusion at some later date (after completion of ATLAS construction) would be greatly complicated. On the other hand, outer chambers (EOL/S) would be the final ones installed and they could in principal be appended after initial running with presumably less "digging up the street" than required for the internal elements.

Due to the need to rapidly produce and disseminate this study we have chosen to run with standalone versions of the MDT simulation, LHCTOR [1] and reconstruction, MUONBOX [2] codes. The former is a GEANT based program which simulating the MDT sensitive detectors and the mass profiles of the internal detectors, magnet and other structural elements. The run parameters of LHCTOR are set to enable δ-ray production and all standard physics processes. Gammas and electrons were tracked to 0.5 Mev, muons to 1 MeV. MUONBOX, after it provides digitization of the LHCTOR produced hits, performs track and momentum reconstruction. The analysis parameters of MUONBOX are intrinsic tube resolution 85μm; random noise hits turned

off. The actual tube resolution coded in MUONBOX is parameterized to yield an impact parameter dependent value which is then sampled from a normal distribution. The geometrical database used is Version K along with Version 1 of the magnetic field. This geometrical description, although not the most recent, is completely adequate for the purposes of this differential type study. A cross check of the baseline configuration using DICE and ATRECON (release 39) (which calls MUONBOX) employing the geometrical description Version M *amdb_simrec.M2.8* and magnetic field Version 2 *bmagatlas02.data* yielded very similar reconstruction rates and resolution.

2 Chamber Configurations

With the above considerations in mind, we have concentrated our investigation on two scenarios that differ from the baseline configuration (as outlined in revision K of the AMDB geometrical description). In the first, the outer chambers have been removed from the simulation (or equivalently, their hits are not written out). These outer chambers are labeled as EOL, EOS, FOL and FOS in database version K, and as EOL and EOS in more recent versions. We regard that the overall geometric definition and positioning of the chambers, while not identical in the two databases, is sufficiently close for the purposes of this study. In Addendum A we present a special case where only the lower rapidity chambers of the outer section are absent: EOL/S 1,2,3 in geometrical database K (or EOL/S 4,5,6 in later versions.) Finally, with the outer chambers in place we remove EEL/S chambers spanning the pseudo-rapidity interval of $1.0 < \eta < 1.34$. This later configuration is motivated by the somewhat redundant nature of these chambers: they reside midway between the inner EIL and middle distance EML chambers over which distance there is a large field integral of several tesla-meters. In Figure 1 are shown the rapidity regions and chambers relevant to this work.

The simulation runs consisted of 5000 generated muons (μ^+ and μ^- in equal numbers) with transverse momenta, P_t, set at 20, 100 or 500 GeV . In all runs the angular range spanned one quadrant in azimuth such that two large (eg., EOL) and two small (eg., EOS) chambers were covered. The rapidity interval was adjusted to correspond to the chambers under review.

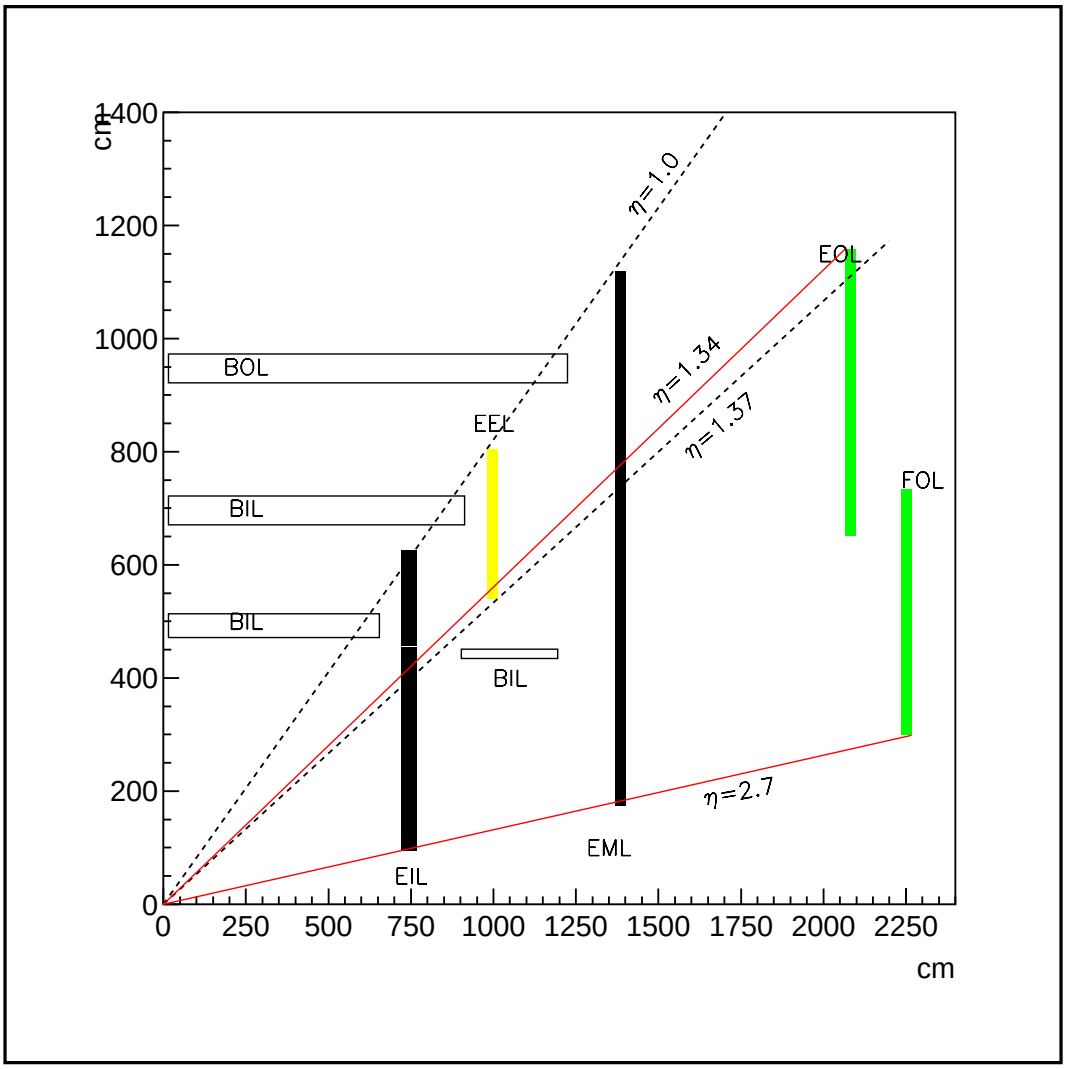

Figure 1: Example of baseline layout of chambers in barrel and end-cap used in this study. Only the large chambers are shown. Positions correspond to geometrical database Version K. The EEL (yellow) and EOL/FOL (green) are alternately left out of the simulations.

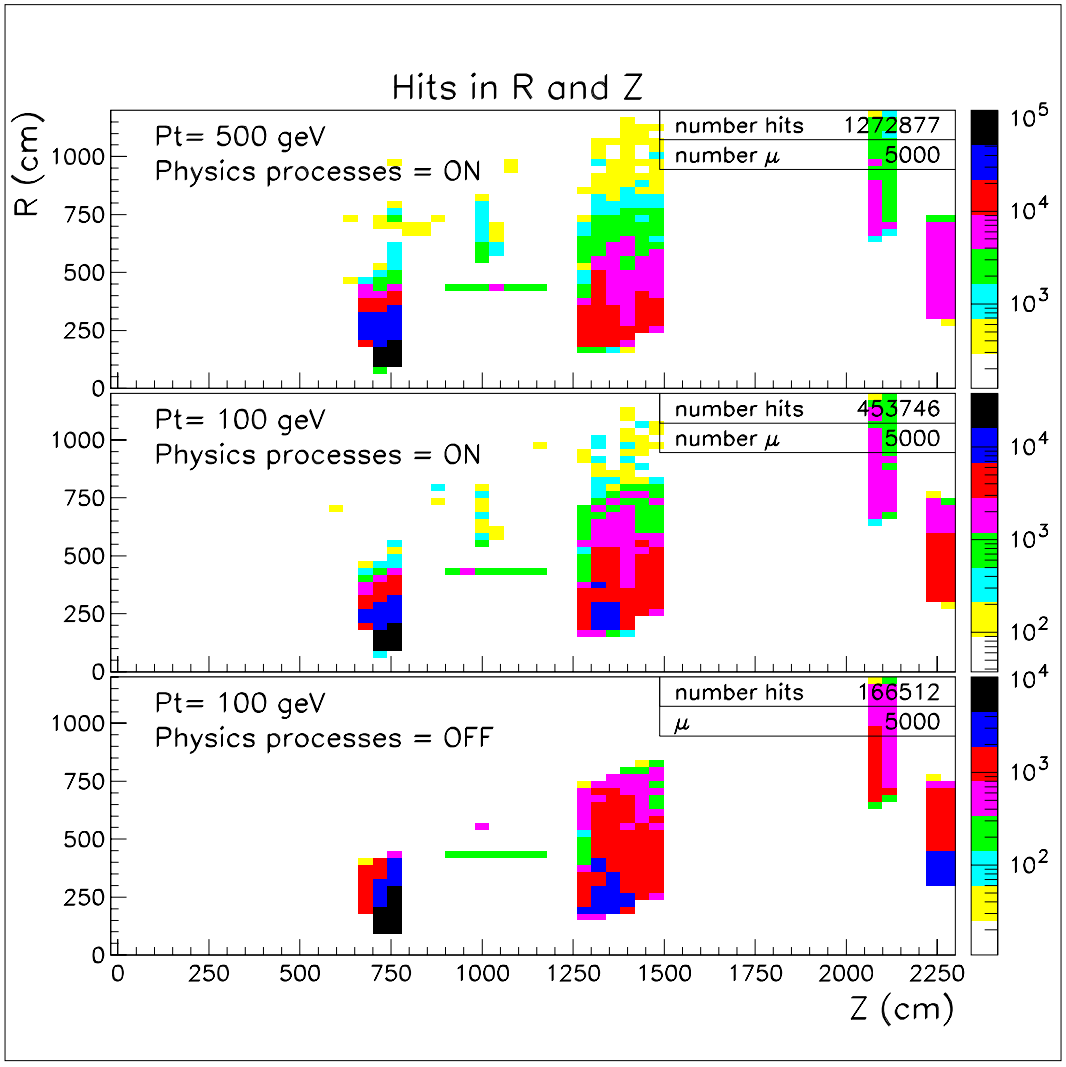

Figure 2: Location and number of hits induced by 5000 muons ($P_t = 100$) with all physics process disabled in GEANT; ($P_t = 100$) with physics enabled; ($P_t = 500$) with physics enabled. The EOL/S and FOL/S chambers are at Z=2150 cm and 2250 respectively.

3 Results I: Single muons, without EOL/S and FOL/S chambers

In these runs the outer chambers (corresponding to EOL/S and FOL/S or EOL/S in database versions K and M respectively) are removed and performance is compared to the baseline. The initial run, with P_t=20 GeV indicates somewhat poorer resolution and several times more unreconstructed tracks than in the baseline case. In Figure 3 are shown the average Gaussian and RMS resolutions for all reconstructed muons in the baseline and truncated schemes. The resolution is significantly poorer with the outer chambers removed. In Figure 4 is plotted the RMS resolution versus the rapidity. At the low end, from η 1.34 to η = 1.6 muons pass through the so-called magnetic transition region where the field integral is nearly zero. This is due to the canceling fields of the barrel and end-cap toroids.It may be expected therefore that the small field integral from the middle to outer chambers assumes a greater weight in momentum determination. The region from 1.6 to 2.0 is spanned by an extension of the barrel system; BEE chambers. This intermediate point helps offset the effect the missing chambers. Beyond this point there are only two chambers participating in the track reconstruction.

Aside from poorer resolution the number of unreconstructed tracks, while not large in either case, increases by about a factor of five in the absence of the outer chambers. This is shown in Figure 6 where the angular locations of the unreconstructed tracks are plotted. The RMS resolution over azimuth, Figure 5, follows the waxing and waning of the field integral but otherwise reveals no additional phi-angle dependence when chambers are removed.

When the P_t is set at 100 GeV the situation worsens as evidenced in Figure 7. Not only is the momentum distribution much broader but now significant non-gaussian tails appear. At these momenta the tracks are much stiffer and can be followed back along an essentially straight trajectory from the middle to outer chambers. This long lever arm constrains the angle of the track vector in the middle chamber. As the error of this angle folds into the error of the momentum determination it is expected that the absence of the outer chambers greatly increases this error; that is, $\delta P/P \sim \delta\theta/\theta$. The resolution smearing at higher rapidity, Figure 8, reflects the fact that θ becomes small.

Further, increased momentum is accompanied by increased delta rays production and EM showering. The multiplicity of particles in the second layer poses a pattern recognition problems best resolved by the presence of the outer

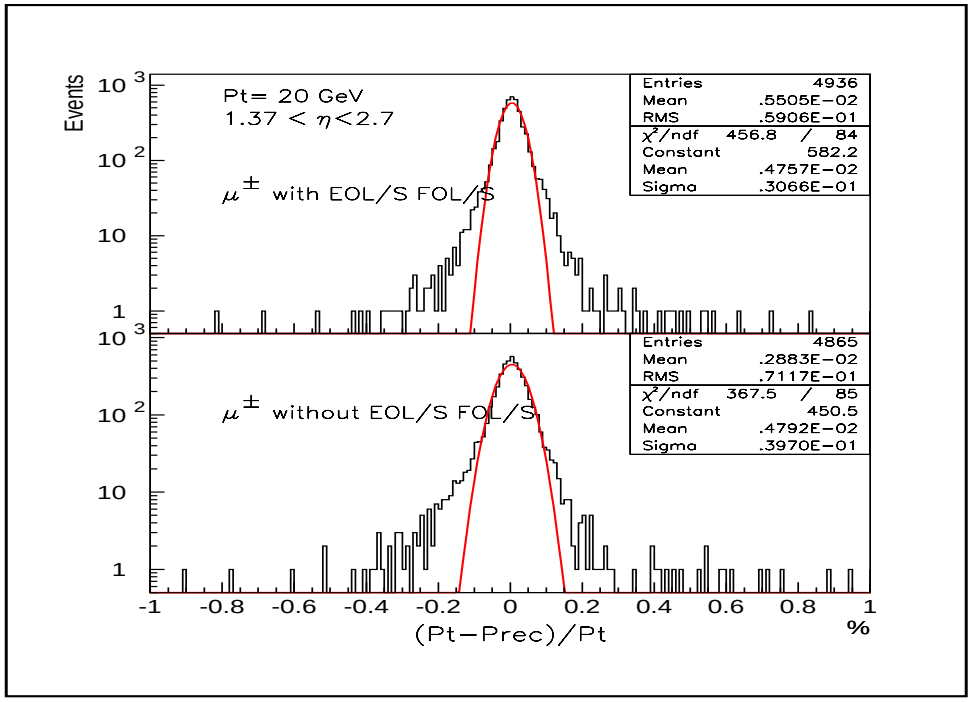

Figure 3: Reconstructed P_t residuals induced by 5000 $\mu^{\pm}$ ($P_t = 20$ GeV) traversing over $1.34 < \eta < 2.71$ and over ± 45 degrees in azimuth. **Top:** Baseline configuration. **Bottom:** Without outer end-cap chambers.

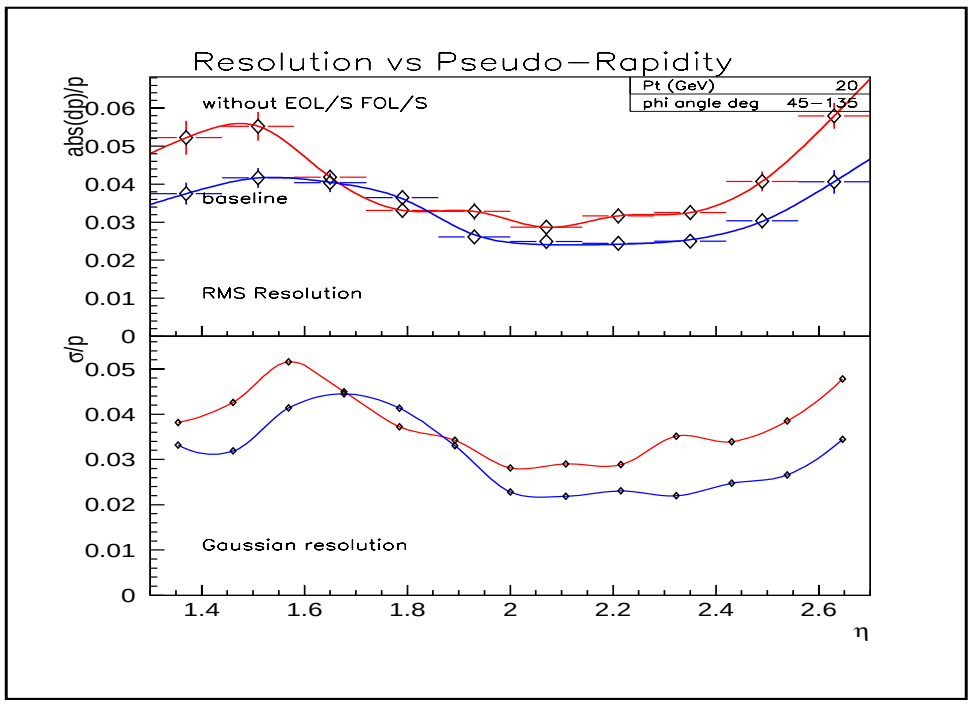

Figure 4: **Top:** Absolute value of P_t residuals versus pseudo-rapidity induced by 5000 $\mu^{\pm}$ ($P_t = 20$ GeV) averaged over ± 45 degrees in azimuth. **Bottom:** Resolution obtained from Gaussian fits to each of 13 projective slices in η.

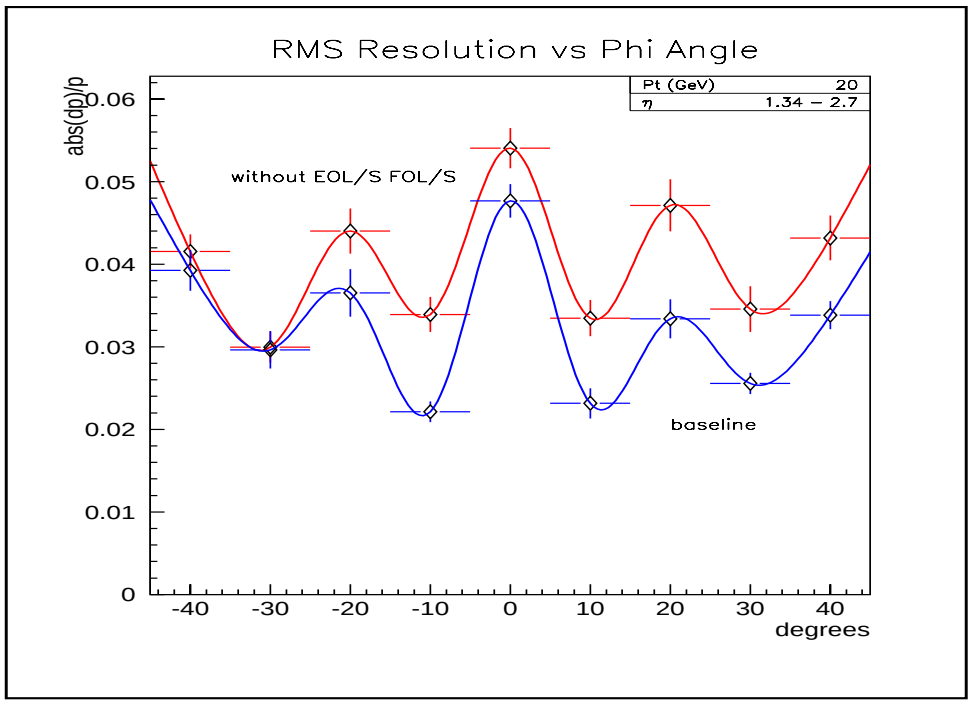

Figure 5: Absolute value of P_t residuals versus azimuth induced by 5000 $\mu^{\pm}$. ($P_t = 20$ GeV) averaged over $1.34 < \eta < 2.71$. The periodic variations reflect the variations in the magnetic field integral.

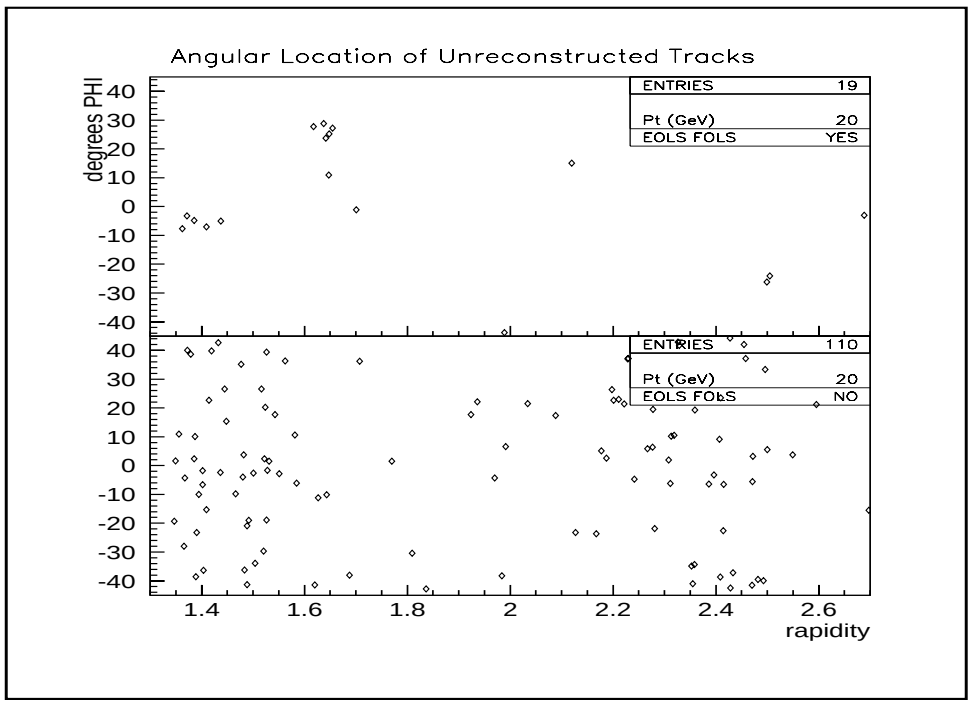

Figure 6: Locations of unreconstructed $P_t = 20$ GeV $\mu^{\pm}$ in $\phi\eta$ space. **top:** Baseline. **Bottom:** Without outer end-cap chambers. The number of unreconstructed tracks, much larger in the bottom plot, represents a 2% acceptance loss. Total sample size is 5000.

trackers. Figure 2 shows the hit pattern and rate for three cases: for 100 GeV "sterile" muons (i.e all physics processes disabled), 100 GeV and 500 GeV with all physics enabled. The associated particle production increases the hit rate by about a factor of three at 100 GeV . Increasing the P_t to 500 GeV yields another factor of 2.5.

To establish the "raw" resolution broadening we perform the comparison using "sterile" 100 GeV runs. In this case there is no pattern recognition problem; every event consists of a single clean track unaccompanied by other charged particles. In Figure 9 and Figure 10 are shown the baseline and *sans* EOL/S FOL/s configurations. While the gaussian resolution is about the same with physics processes turned on, the absence of tails is notable and the number unreconstructed tracks is reduced from 60 to 19. The resolution dependence on η also changes little from the "physics enabled" case. From this we conclude that the outer chambers are required not only to alleviate pattern recognition complexity, but to provide adequate momentum measurement even in the complete absence of spurious hits.

At P_t=500 GeV the number of hits (due to charged particles) in the chambers is about seven times generated by the muon alone. Without the outer chambers, pattern recognition is severely compromised and the momentum residuals distribution (Figure 11) is non-Gaussian and is broad at all rapidities, (Figure 12).

4 Results II: Single muons, without EEL/S chambers

With the EEL/S midsection chambers removed (and outer section chambers in place) sets of 5000 single muons at 20 and 100 GeV P_t have been propagated over the range $1 < \eta < 1.37$. At 20 GeV the average resolution degrades from about 2% to 3% Figure 13, mostly in the η regions removed from overlap with barrel chambers, Figure 14. The number of events that fail to reconstruct increases (Figure 15). Many of these missed events cluster at the lower EES chamber extremities where there is a gap in the FIS/BIS coverage[6].

Given that the EEL/S chambers reside in a large field integral region, their contribution to the momentum resolution and is important. Just how important is revealed in Figure 16 in which restricted Gaussian fits are shown. Resolution versus η is shown in Figure 17. The two cases converge at the extrema ($\eta = 1$ and $\eta = 1.4$) where tracks clip the barrel chambers (BEE, BIL,

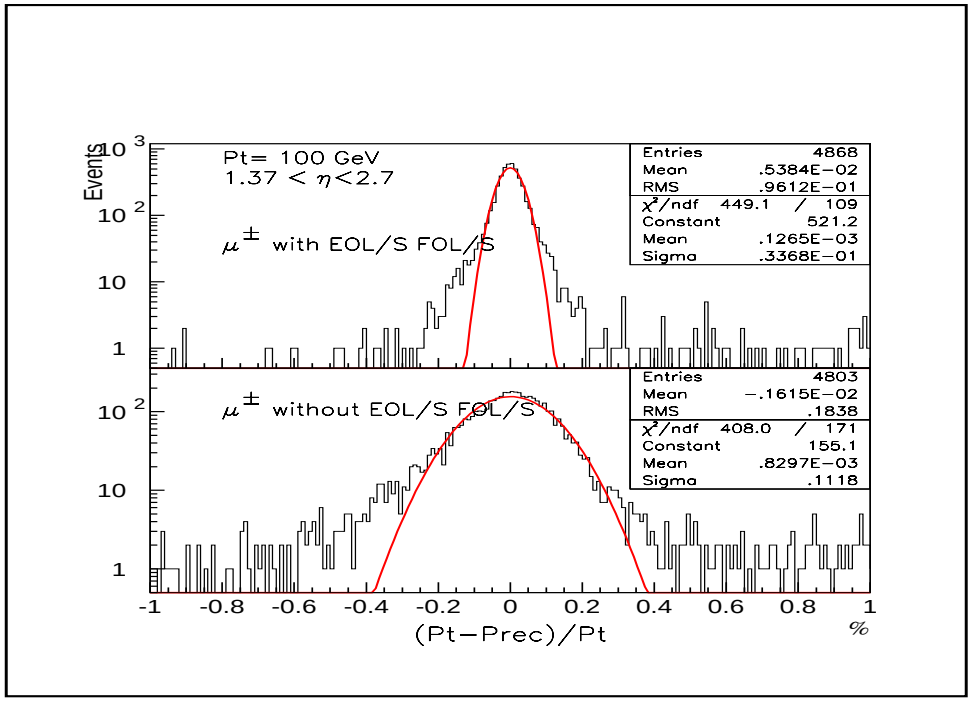

Figure 7: Reconstructed P_t residuals induced by 5000 $\mu^{\pm}$ (P_t = 100 GeV) traversing over $1.34 < \eta < 2.71$ and over ± 45 degrees in azimuth. **Top:** Baseline. **Bottom:** Without outer end-cap chambers.

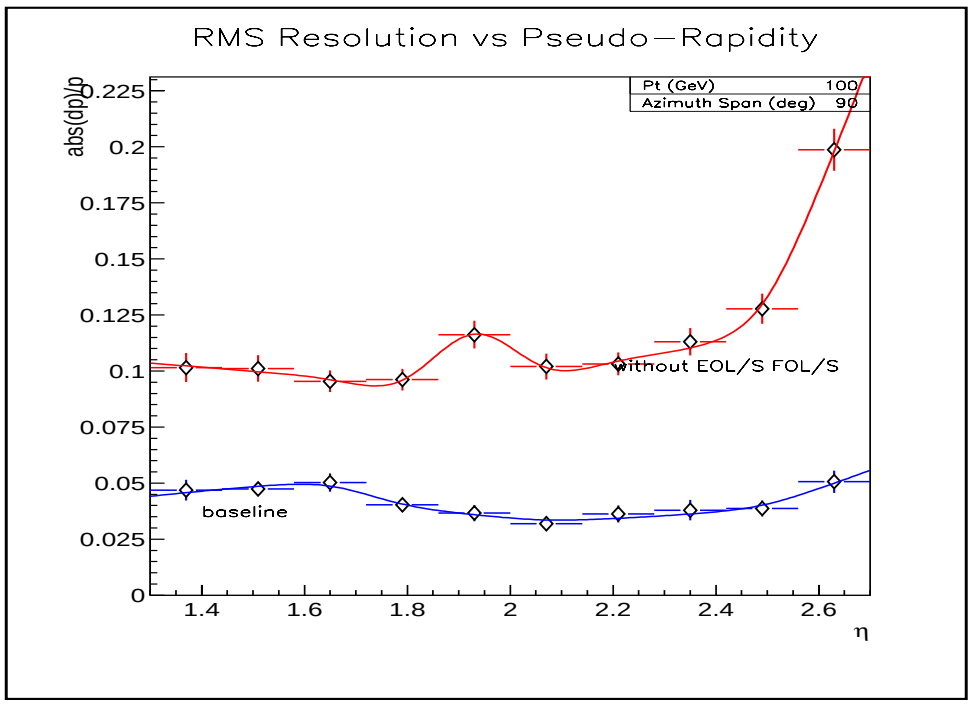

Figure 8: Absolute value of P_t residuals versus pseudo-rapidity induced by 5000 $\mu^{\pm}$ (P_t = 100 GeV) averaged over ± 45 degrees in azimuth. Upper line: Without outer end-cap chambers. Lower line: Baseline.

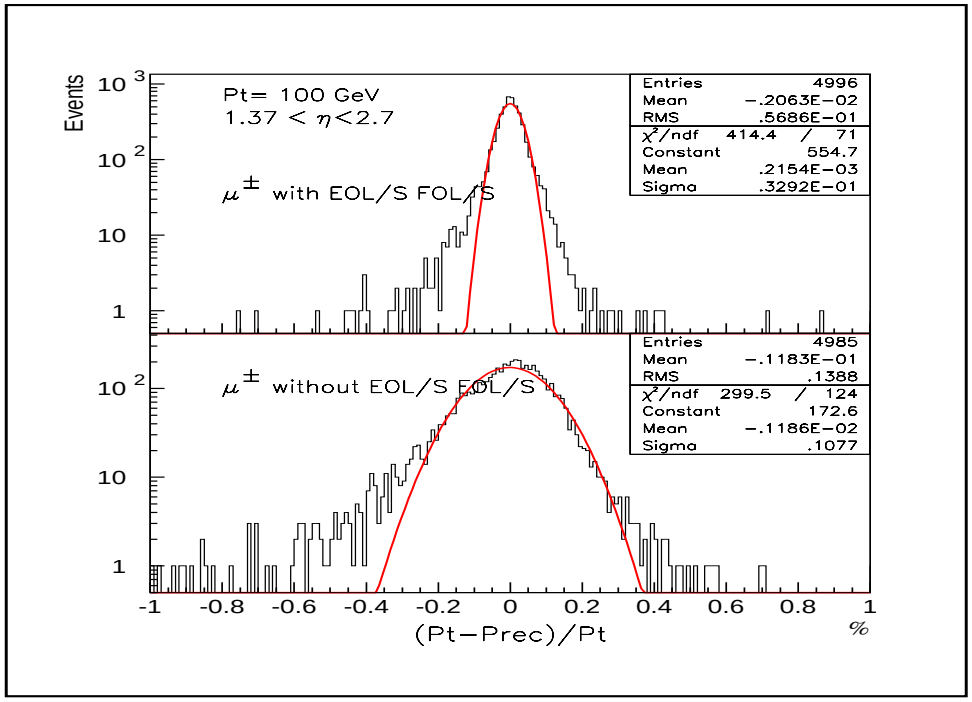

Figure 9: Reconstructed P_t residual for "sterile" muons, i.e. all physics processes disabled. Data are from 5000 $\mu^{\pm}$ (P_t = 100 GeV) traversing over $1.34 < \eta < 2.71$ and over ± 45 degrees in azimuth. In this data set all physics process have been disabled.
Top: Baseline. **Bottom:** Without outer end-cap chambers.

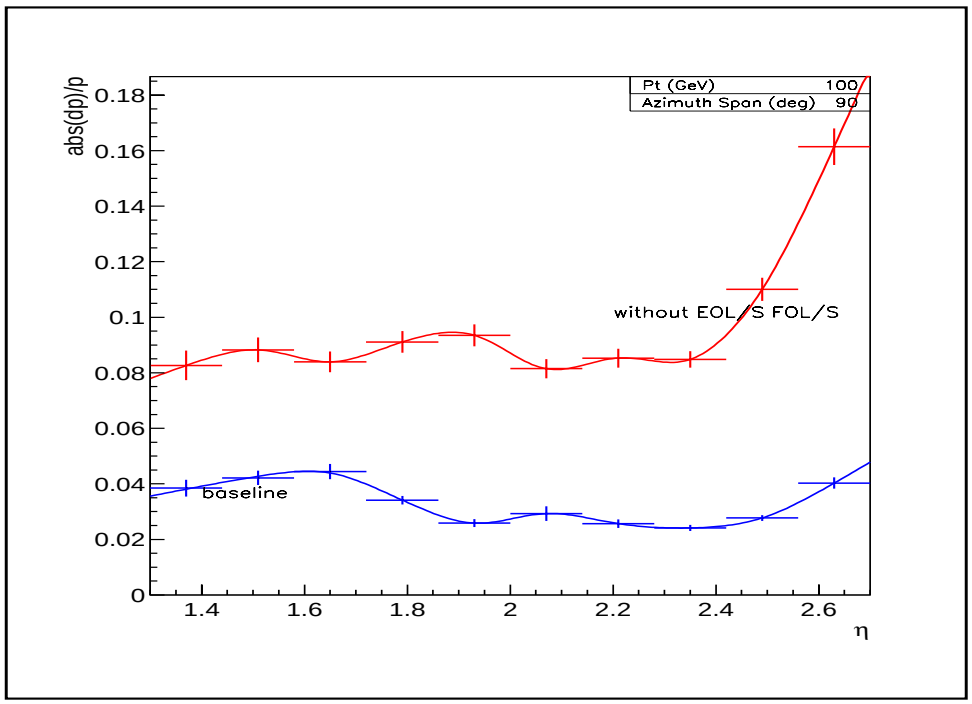

Figure 10: Absolute value of P_t residuals versus pseudo-rapidity for "sterile" muons, i.e. all physics processes disabled, induced by 5000 $\mu^{\pm}$ (P_t = 20 GeV) averaged over ± 45 degrees in azimuth. Upper line: Without outer end-cap chambers. Lower line: Baseline.

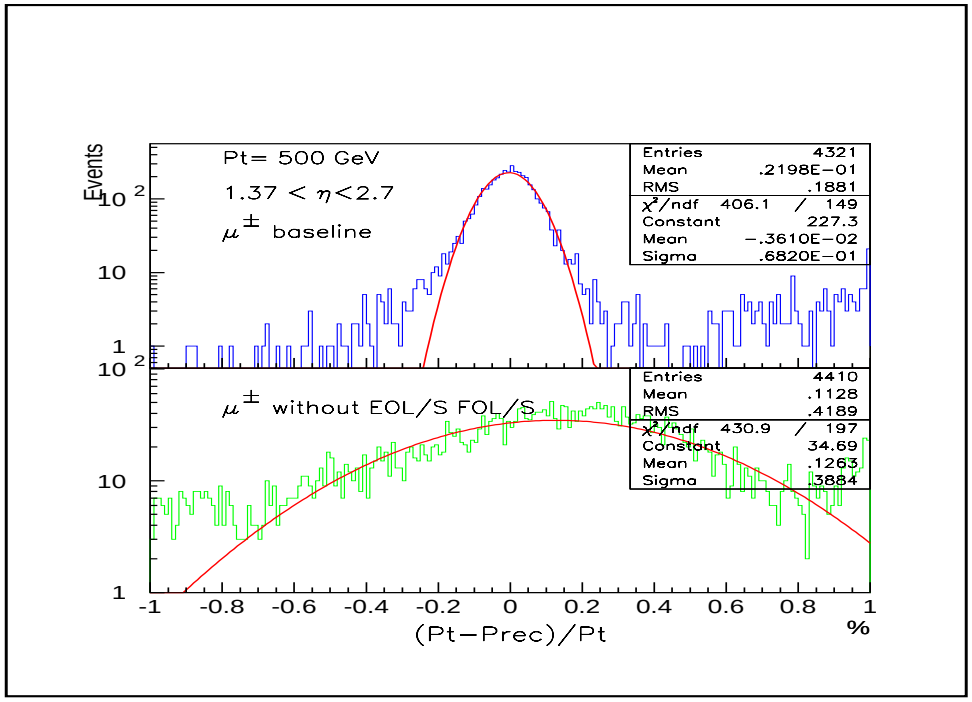

Figure 11: Reconstructed P_t residuals induced by 5000 $\mu^{\pm}$ (P_t = 500 GeV) traversing over $1.34 < \eta < 2.71$ and over ± 45 degrees in azimuth. **top:** Baseline. **Bottom:** Without outer end-cap chambers.

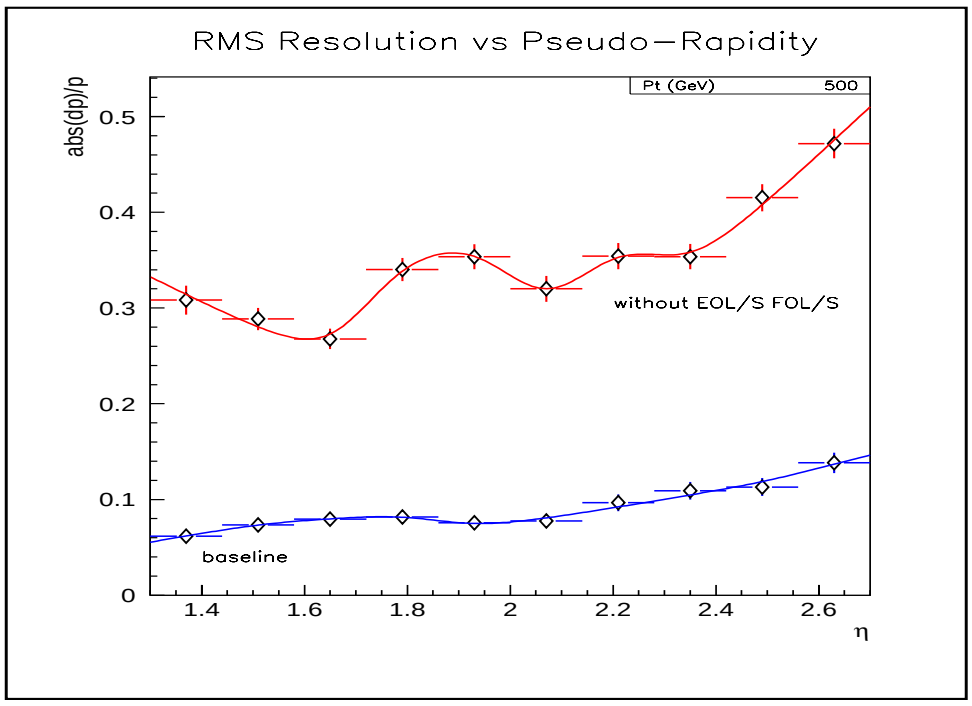

Figure 12: Absolute value of P_t residuals versus pseudo-rapidity induced by 5000 $\mu^{\pm}$ (P_t = 500 GeV) averaged over ± 45 degrees in azimuth. Upper line: Without outer end-cap chambers. Lower line: Baseline.

BML, BOL) and the endcap FIS chambers. At this momentum the Gaussian resolution is degraded from .02 to .0326, but the increase in non-gaussian tails is dramatic. The number of events in the tails (more than 3σ from the center) is 372 and 966 for the baseline and missing EEL/S cases respectively.

5 Higgs Mass Resolution

With some idea on how the single muon momentum resolution is affected by the absence of a third track vector we proceed to assess the reconstruction of a Higgs mass for the 4 muon decay,

$$H^0 \rightarrow Z^0 Z^* \rightarrow \mu^+\mu^-\mu^+\mu^-$$

at masses of 150, 200 and 500 GeV . We will evaluate only the scenario in which the EOL/S FOL/S chambers are not installed. The Higgs decay to the 4-muon final state is generated using PYTHIA[8]. The detector simulation, digitization and muon momentum reconstruction proceed exactly as in the single muon case above. A final analysis step extracts the reconstructed muons from MUONBOX and calculates the invariant mass from all candidate pairs. This procedure is augmented by using a mass constraint; the muon pair whose 4-momentum squared is closest to the Z^0 invariant mass is first identified.

Here we consider that the width of the fitted mass peak (σ_{fit}/M_{fit}) is essentially the quadratic sum of the intrinsic width of the Higgs σ_H and the average momentum resolution, $< dp/p >$:

$$\sigma_{fit}(p)/M_{fit} = ((\sigma_H(M_H)/M_H)^2 + < \sigma_p/p >^2))^{1/2} \quad (1)$$

where $< \sigma_p/p >$ is averaged over rapidity and azimuthal angle. In particular we estimate:

$$\int_{Barrel} f(M_H,\eta)\sigma_p(\eta)d\eta + \int_{end-cap} f(p,\eta)\sigma_p(\eta)d\eta \quad (2)$$

where $f(p,\eta)$ is the fraction of muons per unit rapidity produced by the decaying Higgs.

With increasing Higgs mass the decay tends to become more isotropic so the probability for muons to traverse the forward EOL/S FOL/S chambers is somewhat reduced. For M_H =150-200 GeV about 33% of the muons pass through this region and is reduced to 27% for M_H=500 GeV .

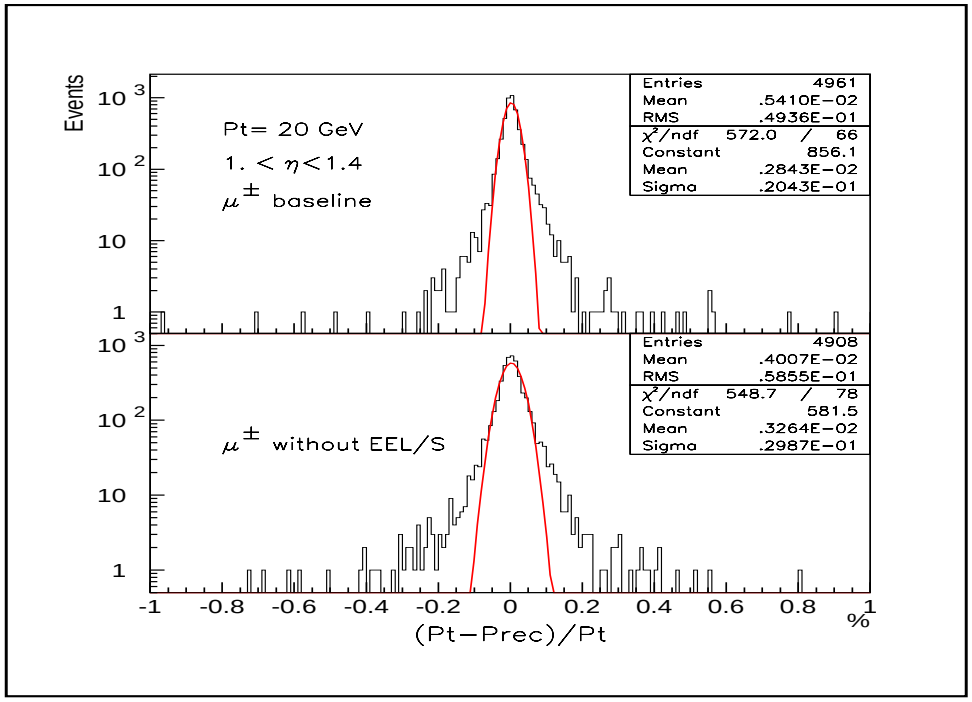

Figure 13: Reconstructed transverse momenta residuals induced by 5000 $\mu^{\pm}$ (P_t = 20 GeV) through the EEL/S region, spanning $1. < \eta < 1.37$ and over ± 45 degrees in azimuth. **Top:** Baseline. **Bottom:** Without outer end-cap chambers.

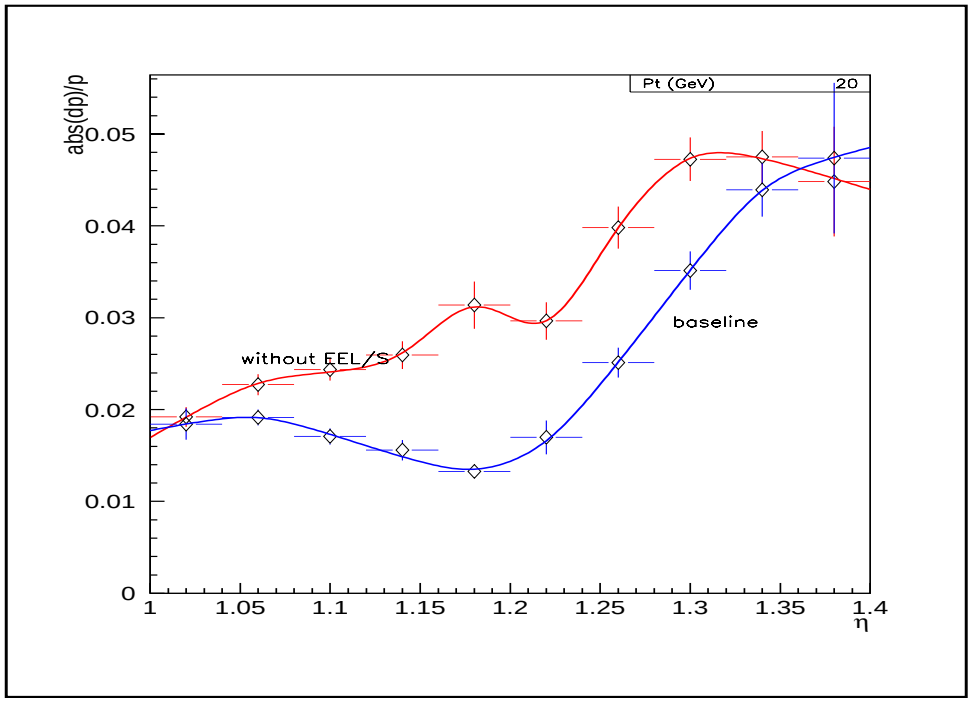

Figure 14: Absolute value P_t residuals in EEL/S chambers versus pseudo-rapidity induced by 5000 $\mu^{\pm}$ (P_t = 20 GeV) averaged over ± 45 degrees in azimuth Upper line: Without outer end-cap chambers. Lower line: Baseline.

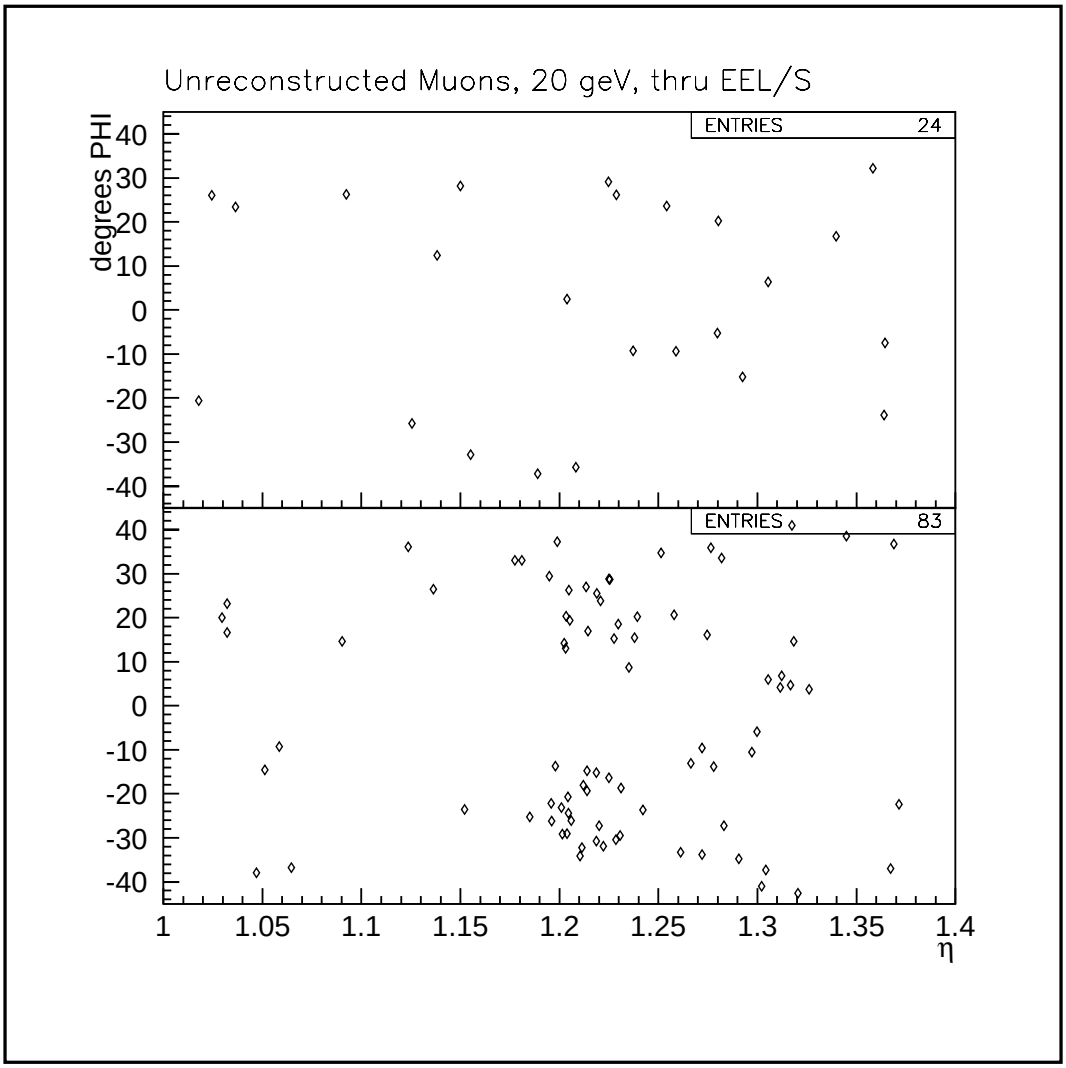

Figure 15: Angular locations of unreconstructed $P_t = 20$ GeV $\mu^{\pm}$ through the EEL/S chambers. Total sample size is 5000. **Top:** Baseline. **Bottom:** Without mid-section chambers: EEL and EES. Note the clustering of missed events reflects an acceptance gap in the small chamber layout corresponding to the corner of FIS and BIS chambers.

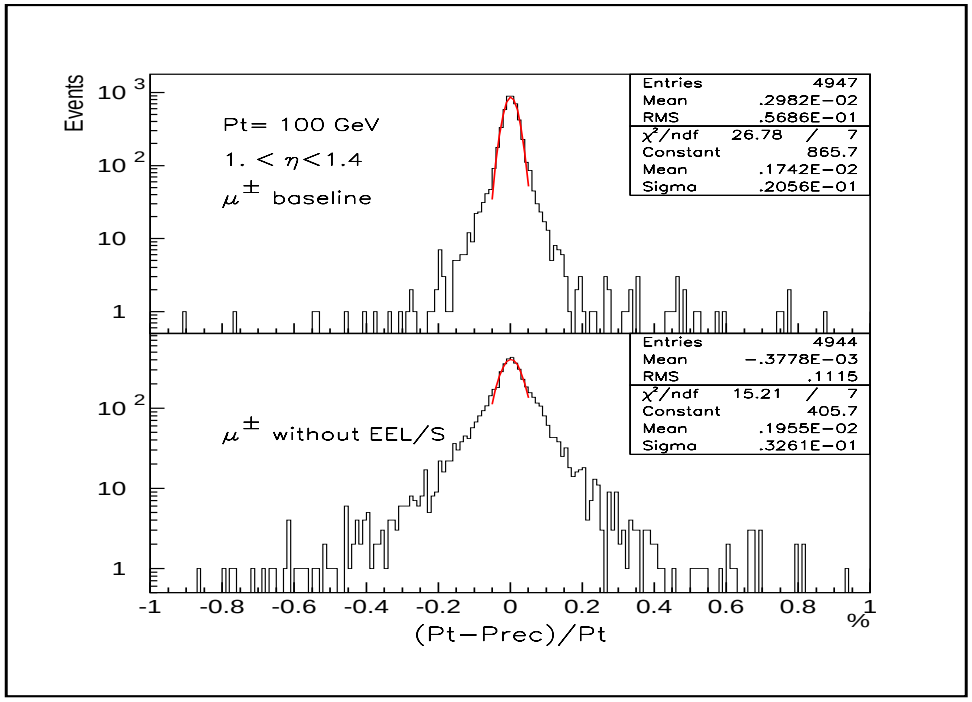

Figure 16: Reconstructed P_T residuals induced by 5000 $\mu^{\pm}$ ($P_t = 100$ GeV) through the EEL/S region, spanning $1. < \eta < 1.37$ and over ± 45 degrees in azimuth. **Top:** Baseline. **Bottom:** Without midsection EEL and EES chambers.

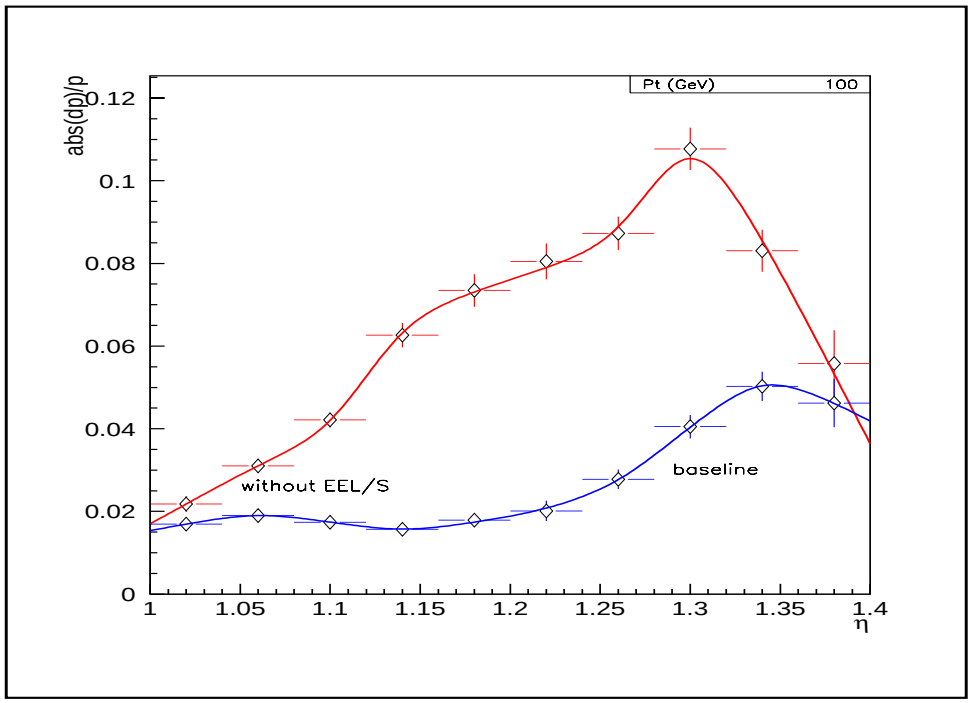

Figure 17: Absolute value P_t residuals in EEL/S chambers versus pseudo-rapidity induced by 5000 $\mu^{\pm}$ ($P_t = 100$ GeV) averaged over ± 45 degrees in azimuth. Upper line: Without midsection end-cap EEL and EES chambers. Lower line: Baseline.

For the purposes of this evaluation the momentum resolution is roughly constant at over the barrel region and increases (but still somewhat flat) over the end-cap. For M_H=150- 500 GeV the average P_t (Figure 18) ranges from 34 to 110 GeV , corresponding to barrel ($\eta < 1.5$) resolution [5] of about 2% and increasing to about 3% in the end-cap. As demonstrated earlier, the endcap (EOL/S FOL/S) momentum resolution degrades from 3.1% to 4% at P_T=20 GeV ($M_H \sim 150$ GeV) and from 3.3% to 11% at P_T=100 GeV ($M_H \sim 500$ GeV). While the loss of resolution is more severe at P_T=100 GeV than at lower P_T, the intrinsic width of the Higgs (Figure 19) increases for larger masses and dominates the smearing of the observed peak. For M_H=150 GeV the intrinsic width is small and the change in the measured width due to the end-cap chamber implementation is apparent. For M_H=500 GeV a small but insignificant width increase is observed, consistent with $\sim$ 1% expected.

In Figure 20 are shown the fit Higgs peaks for M_H = 150, 200 and 500 GeV with and without the EOL/S and FOLS/S chambers in place. From 1 the expected change in the fit peak width is from 2.4% to 2.7% for M_H=150 GeV. This corresponds to about a 12% broadening, in general agreement with the 15% increase obtained.

While no significant change in gaussian width caused by the absence of EOLS/FOLS chambers is seen for M_H=500 GeV , the number of events on the tails ($> \pm 2\sigma$) increases from 363 (out of 1888 4-muon events) to 414 (out of 1872 4-muon events), or an 11% decrease of events under the peak. This is expected from increased pattern recognition complexity at higher momenta. At 150 and 200 GeV the change in the number of outliers is not significant.

5.1 Summary

The increase in muon momentum error arising from a two rather than three chamber measurement results in a $\sim$ 15% broadening of the Higgs mass peak for M_H=150 GeV . No increase in outliers is seen. The fraction of events in which at least 4 muons are reconstructed decreases slightly from 78% to 76%. At M_H=500 GeV there is no significant increase in width nor is there a change in the number of fully reconstructed events.

We present in Addendum A a special case where only the EOL/S chambers ($1.37 < \eta < 1.87$) are absent and the FOL/S remain in place. The results from this study indicate a marginal average loss of resolution at P_t = 20 GeV from 0.039 to 0.041. There is no increase in the non-gaussian tails althought the number of unreconstructed events increased from 29 to 157. This represents

an acceptance loss of about 2% over this limited rapidity region.

6 Conclusion

We have demonstrated that if either end-cap outer (EOL/s) or midsection (EEL/S) chambers are removed then over the P_t range from 20-500 GeV the momentum resolution is degraded over most of the angular acceptance. Furthermore both the number of unreconstructed tracks and the occupancy of non-Gaussian tails increases significantly. As the momentum increases the presence of a third measuring station not only contributes to the improvement of the intrinsic resolution, but contributes to pattern recognition in the presence of many spurious hits accompanying the muon.

This resolution change results in a 15% wider mass peak for Higgs masses near 150 GeV. Calculations of signal over background [7] indicate that the discovery potential for $10^5 pb^{-1}$ (2 years running) depends critically on the Higgs mass and ranges from a maximum of 17.6σ for M_H=150 GeV to 6.0σ at 130 GeV and 5.1σ at M_H=170 GeV . Unless the runtime is appropriately increased, the increased background admitted by a wider mass peak could erode a possible signal into marginality.

As noted in Addendum A the results from the limited case in which only the EOL/S ($1.37 < \eta < 1.87$) chambers are absent and the FOL/S in place (or equivalently in geometrical database versions M and later EOL/S 1,2,3 in place and EOL/S 4,5,6 absent) indicate at most a minor impact on 150-300 GeV Higgs sensitivity. We conclude with the following initial staging scenario which can minimize short term performance loss while facilitating later installation of additional chambers. First we enumerate the current baseline chamber distribution:

1. $2(\pm\eta) \times 3(rings) \times 16$ (chambers/ring) = 96 EIL/S (US) chambers
2. $2(\pm\eta) \times 2(rings) \times 16$ (chambers/ring) = 64 EEL/S (US) chambers
3. $2(\pm\eta) \times 5(rings) \times 16$ (chambers/ring) =160 EML/S (US) chambers
4. $2(\pm\eta) \times 6(rings) \times 16$ (chambers/ring) =192 EOL/S (Rus) chambers

This list specifies 320 US-made chambers of which the delivery of 240 is committed. However the momentum resolution in rapidity region by spanned by the upper (Russian) EOL/S chambers $1.4 < \eta < 2.0$ appears to be least

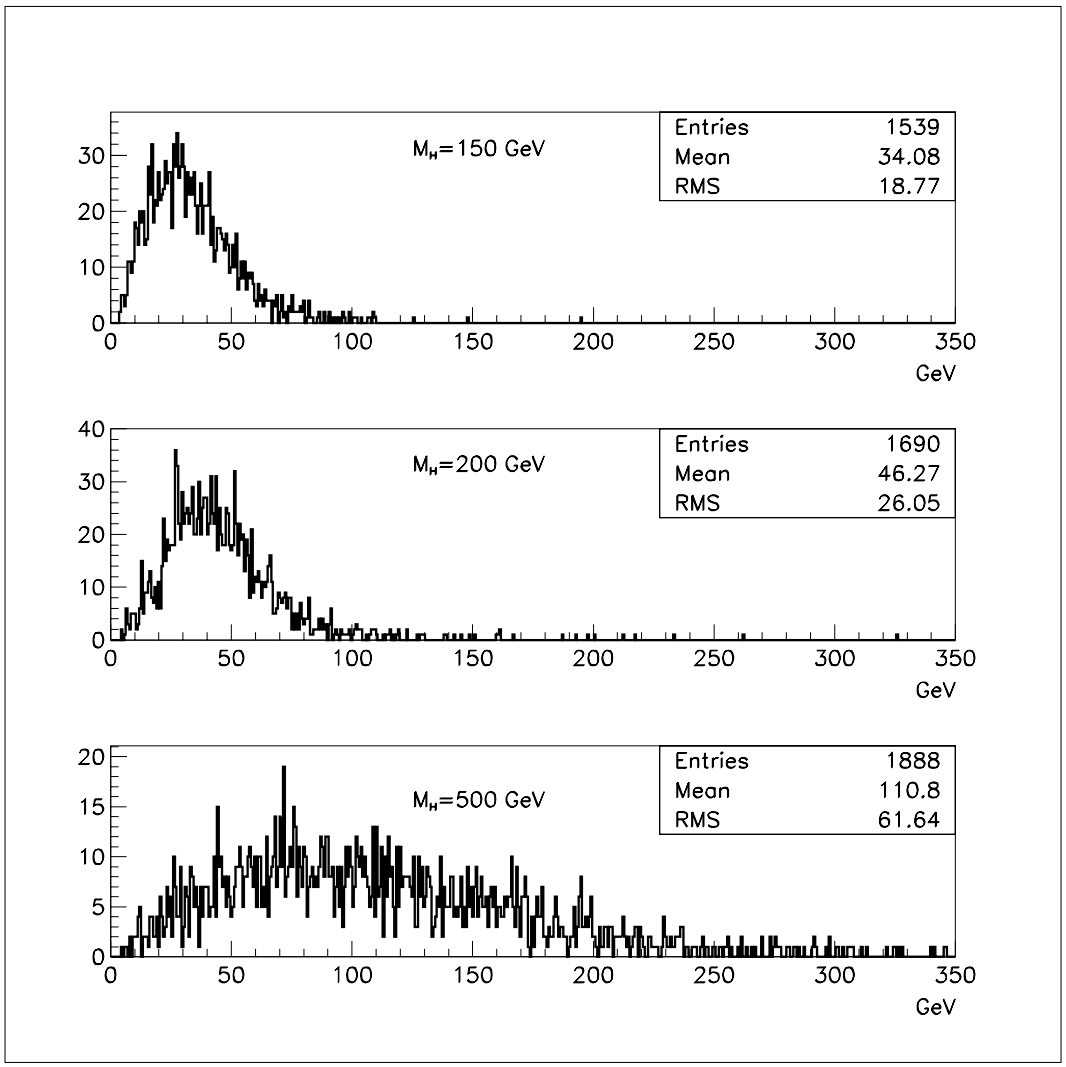

Figure 18: P_t distribution of muons from the decay of 150, 200, 500 GeV Higgs masses.

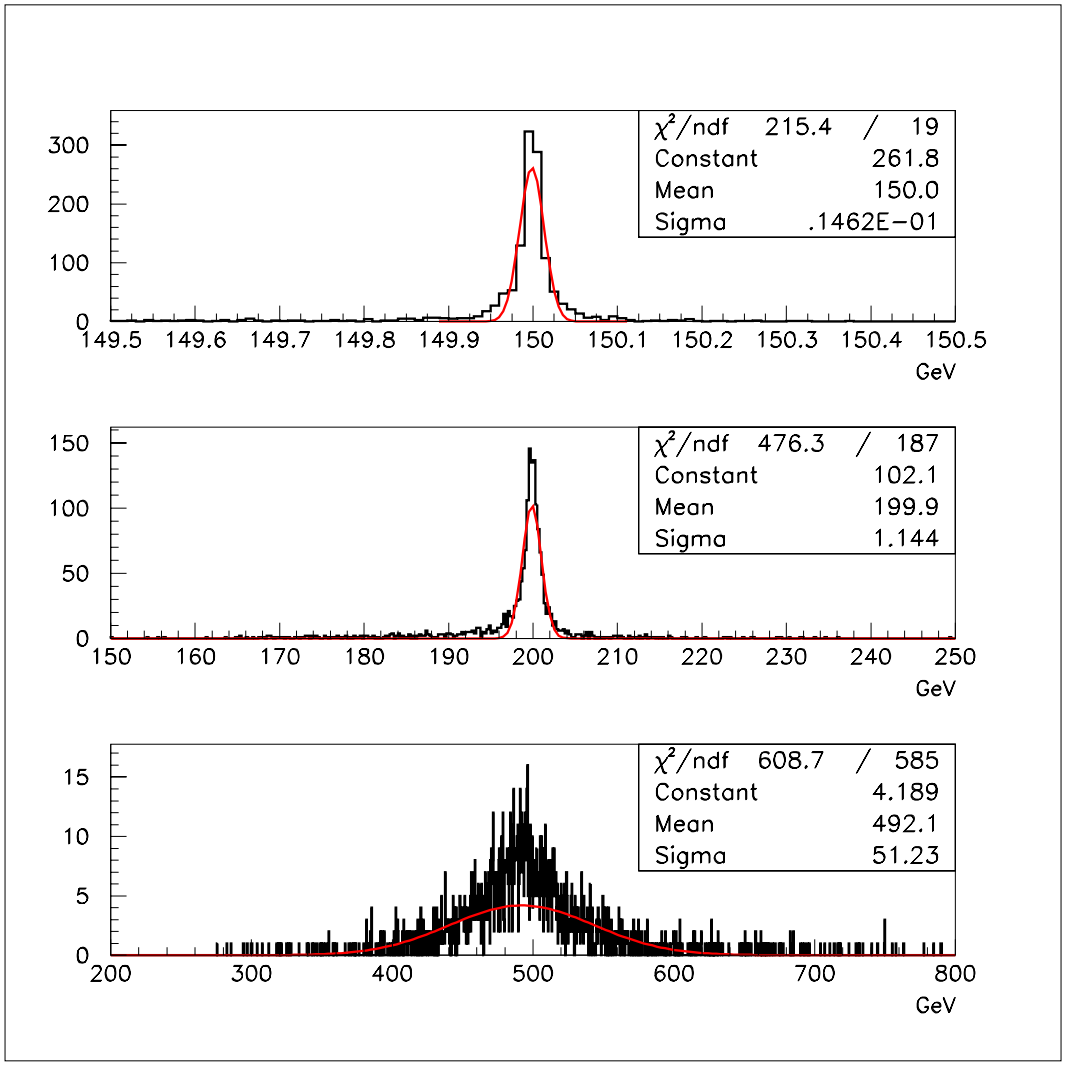

Figure 19: Intrinsic width of 150, 200, 500 GeV Higgs masses. Data are generated by PYTHIA.

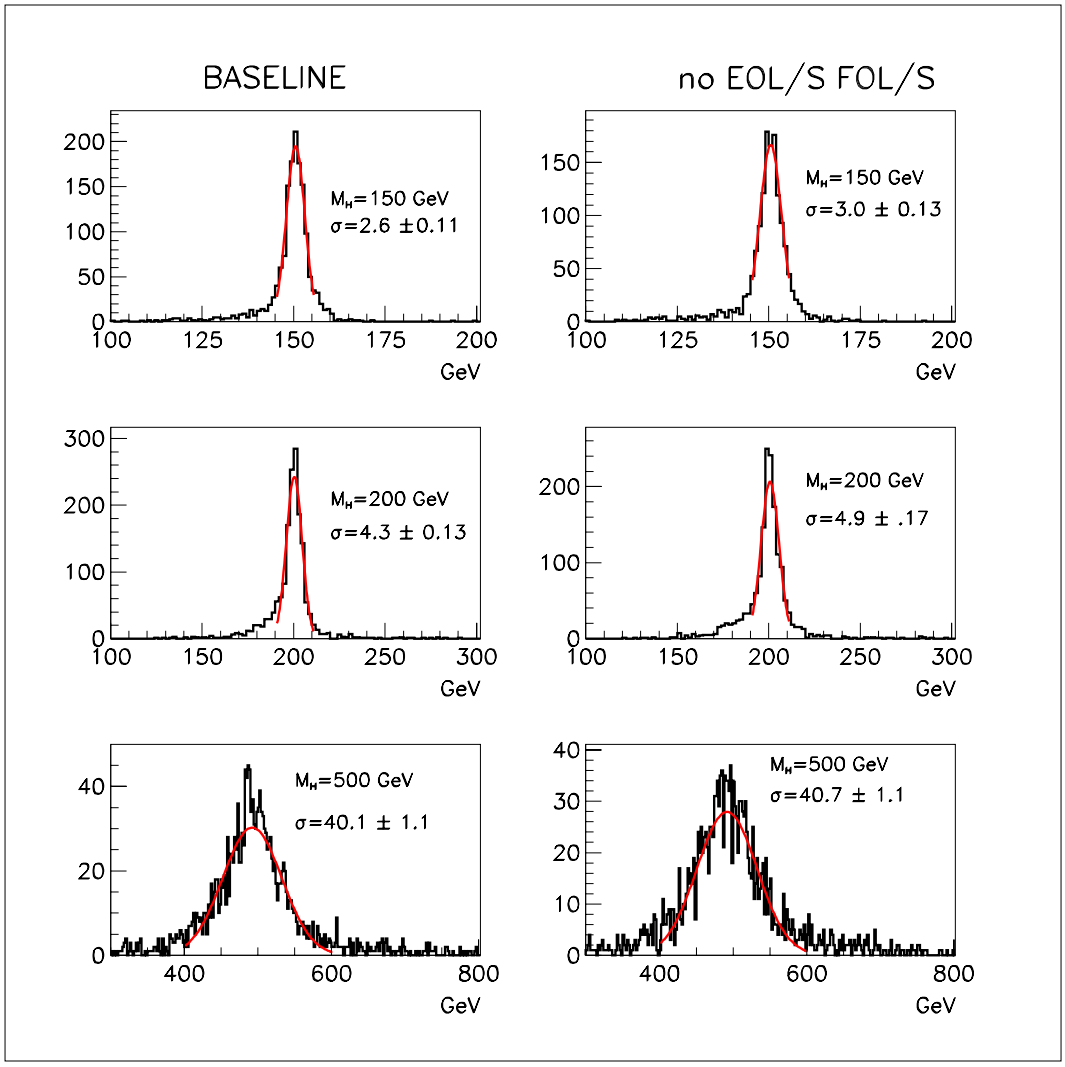

Figure 20: Reconstructed Higgs masses from 4-muon decay of 150, 200, 500 GeV Higgs. Left side is baseline. Right side is with EOL/S FOL/S chambers removed.

sensitive their absence, at least at the $P_t \sim 20$ GeV regime. As noted earlier this is probably due in large part to the redundancy provided by the BEE chambers. We therefore can envision a staging sequence in which production/installation of these 96 chambers is shifted to a lower priority relative to the other end-cap units. It follows that Russian facilities might manufacture the 64 mid-section (EEL/S) chambers and a number of EML/S chambers to make up the difference between the baseline design and the currently approved US commitment. The upper EOL/S chambers would then be assembled and integrated at a later date. From a cursory engineering viewpoint these large radius EOL/S chambers could be installed with relatively less disruption than possibly any other set of end-cap chambers.

7 Addendum A: Without EOL/S

In these runs the outer chambers (corresponding to EOL/S 1,2,3 or EOL/S 4,5,6 in database versions K and M respectively) have been removed from the simulation and performance is compared to the baseline. A dedicated run at with P_t=20 GeV over the corresponding rapidity region ($1.37 < \eta < 1.87$) shows that at these momenta there is only marginal degradation to the average resolution (Figure ??). This degradation occurs in the rapidity interval $1.4\eta 1.6$ corresponding to the magnetic field transition region as shown in Figure4.

As in the case where the entire outer section is missing the number of unreconstructed tracks, while not large, increases by about a factor of five in the absence of the outer chambers. The increase from 29 to 157 in unreconstructed events translates into a 2% loss of acceptance. These events are shown in Figure 22 where the angular locations of the unreconstructed tracks are plotted.

Two runs of about 2400 events for 4 muon Higgs decay have been performed for masses of 150 and 300 GeV. The typical transverse momenta of the muons lies in the 20 -100 GeV range. We therefore expect that the sensitivity be no worse than the earlier case in which the entire end-section (EOL/S FOL/S) is not installed. Indeed as shown in Figure23 there is a slight increase in the observed width of the 150 GeV mass peak from 2.56 to 2.7 GeV. This increase is less than $2\sigma_{fit}$ significance where σ_{fit} is the quadratic sum of the fit width errors. At 300 GeV, due to the increased intrinsic peak width there is no significantly observable change in detection sensitivity.

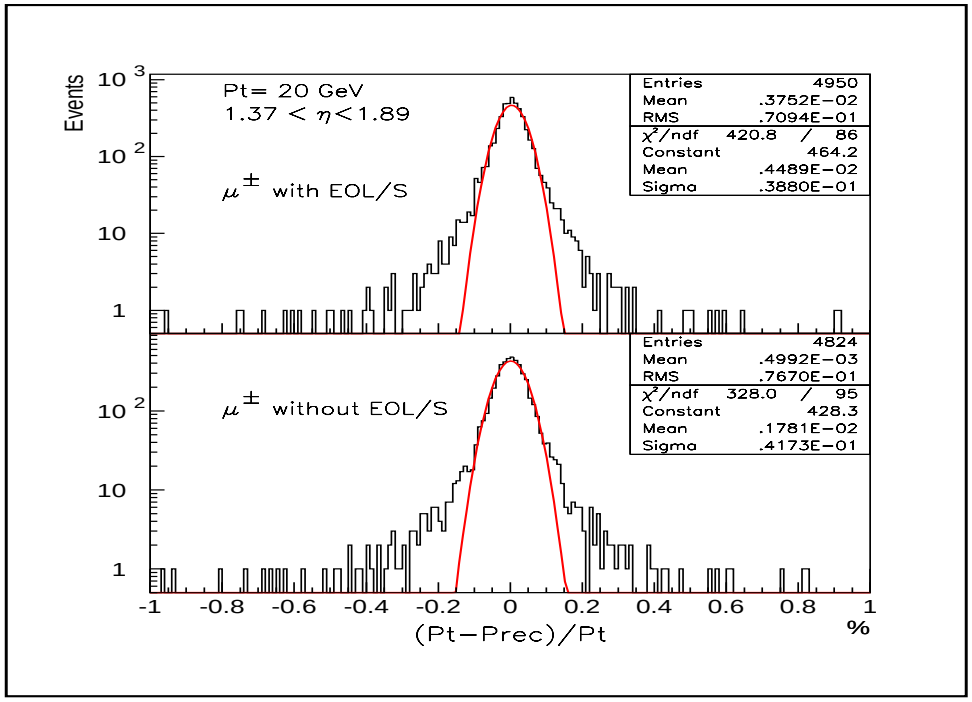

Figure 21: Reconstructed P_t residuals induced by 5000 $\mu^{\pm}$ ($P_t = 20$ GeV) traversing over $1.34 < \eta < 2.71$ and over ± 45 degrees in azimuth. **Top:** Baseline configuration. **Bottom:** Without outer end-cap chambers.

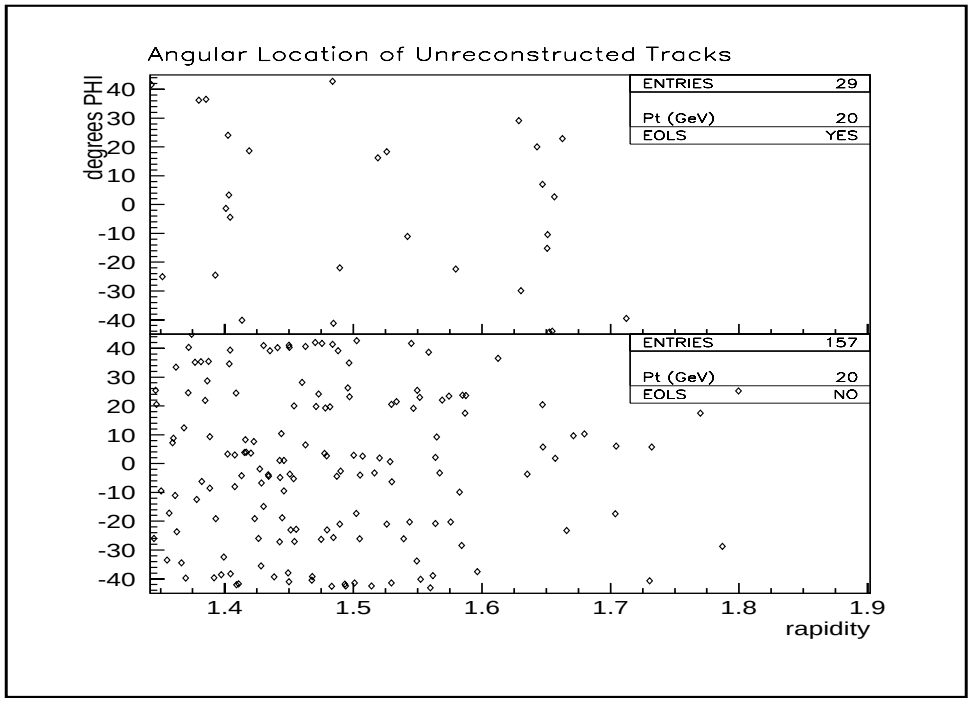

Figure 22: Locations of unreconstructed $P_t = 20$ GeV $\mu^{\pm}$ in $\phi\eta$ space. **top:** Baseline. **Bottom:** Without outer end-cap chambers EOL/S. The number of unreconstructed tracks, much larger in the bottom plot, represents a 2% acceptance loss. Total sample size is 5000.

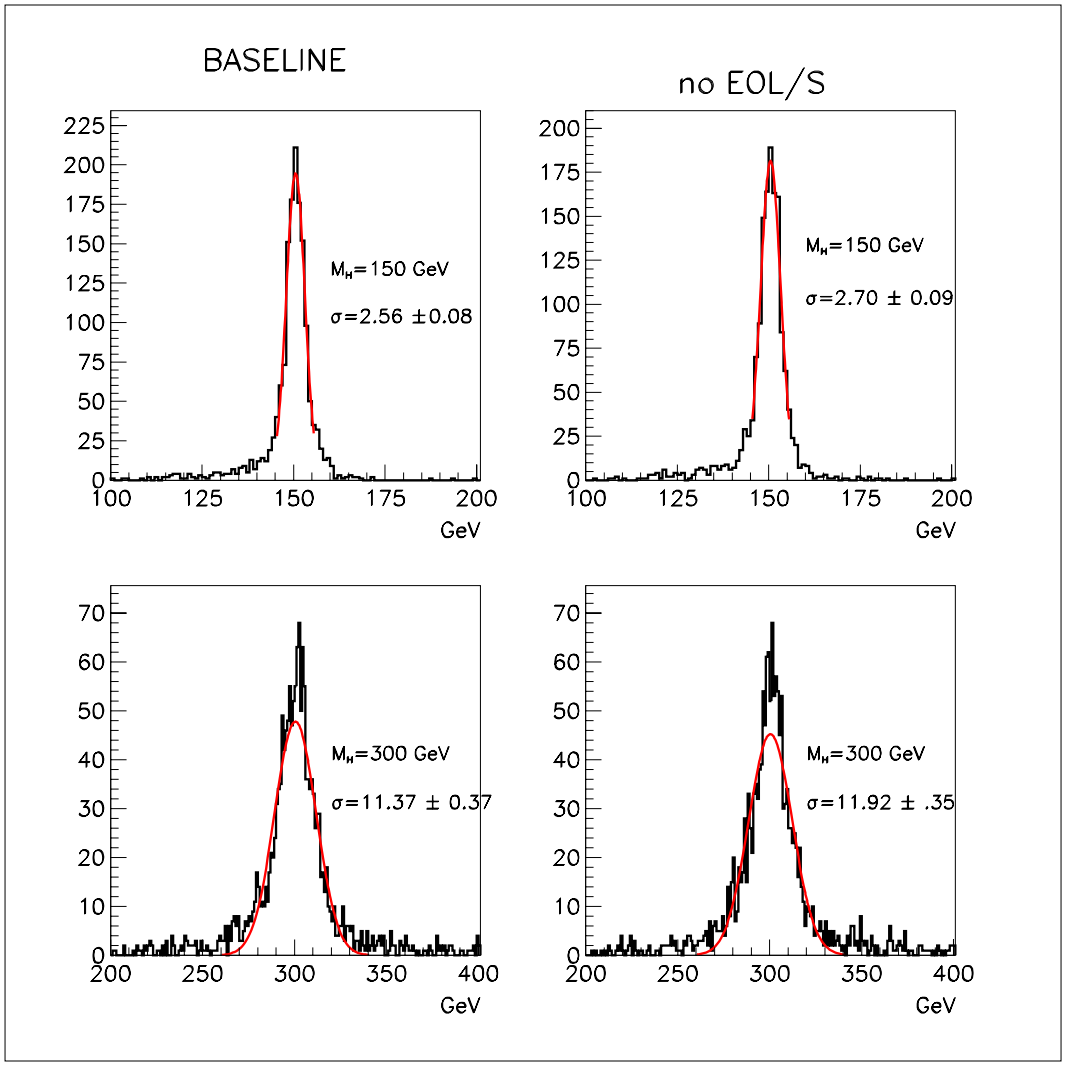

Figure 23: Reconstructed Higgs masses from 4-muon decay of 150, 300 GeV Higgs. Left side is baseline. Right side is with EOL/S chambers removed.

References

[1] L. Chevalier et al, "A Standalone GEANT Program for Simulation of the ATLAS Spectrometer" *ATL-MUON-97-147*, Jul., 1993

[2] M.Virchaux et al, "Muonbox: a full 3D tracking programme for Muon reconstruction in the ATLAS Spectrometer " *ATL-MUON-97-198*, 1997

[3] Revised US ATLAS Project Managment Plan, Appendix 3 available via

`http://www.usatlas.bnl.gov/mgmt/proj-mgmt-plan/proj-mgmt-plan.html`

[4] Revised US ATLAS Project Managment Plan, Appendix 2 available via

`http://www.usatlas.bnl.gov/mgmt/proj-mgmt-plan/proj-mgmt-plan.html`

[5] ATLAS Muon Spectrometer Technical Design Report, page 27 *CERN/lhcc/97-22*, May 31, 1997

[6] ATLAS Muon Spectrometer Technical Design Report, page 70 *CERN/lhcc/97-22*, May 31, 1997

[7] L. Poggioli, J. Shank, K. Sliwa, F. Taylor, T. Trefzger, B. Zhou *ATL-PHYS-98-116* , Jan, 1998

[8] "PYTHIA 5.7 and JETSET 7.4" CERN-TH. 7112/93